CFD STUDY OF THE VOLATILE YIELD EFFECT ON THE PLASMA-ASSISTED BIOMASS GASIFICATION IN A VERTICAL ENTRAINED-FLOW GASIFIER

Robert Lewtak[1]*, Jonas Brandstetter[1], Sebastian Bastek[1], Johannes Waßmuth[1], Kentaro Umeki[1], Andrius Tamosiunas[1], Sebastian Fendt[1], Hartmut Spliethoff[1]

[1] Technical University of Munich, Institute for Energy Systems, Boltzmannstr. 15, 85748 Garching, Germany

*Corresponding Author: robert.lewtak@tum.de

ABSTRACT

The paper presents the results of numerical investigations of the plasma-assisted gasification in an entrained flow reactor. The computations were carried out for varying value of the Q factor that can be achieved by changing the residence time of feedstock in the plasma area. The gasifier mainly acts as a steam reforming reactor. Application of a higher value of the Q factor results in higher quality of the syngas and overall higher gasification efficiency is achieved as well.

1 INTRODUCTION

Advanced gasification technologies such as plasma-assisted gasification processes are a possible solution. They make it possible to process a wide range of potential types of feedstock into high quality syngas for use in chemicals production. For these technologies, possible inputs can be anything from different types of biogenic residues to various hazardous waste streams. During the treatment process, the feedstocks are broken down into basic molecules, e.g., mainly H_2 and CO in the gas phase, at high temperatures. The resulting gasification products can be used to produce a wide range of chemicals through various synthesis processes. The utilization of high temperature plasma in the gasification stage makes it possible to achieve very high carbon conversion efficiencies and while also enabling the addition of high temperature steam for a high share of hydrogen in the final syngas. Thus, plasma-assisted gasification is an attractive option for closing the carbon cycle in a circular economy and is the most popular and cheapest method of hydrogen production, compared to, for example, water electrolysis, the amount of hydrogen obtained per unit of energy consumed is much greater.

2 METHODOLOGY – EXPERIMENTAL SETUP

The experiments to validate the CFD model are conducted in an autothermal pilot-scale entrained flow gasifier, as shown in Figure 1. The gasifier has a fuel input power of around 100 kW and can be separated into three zones. The upper zone where the burner is located, the central zone which contains the reaction chamber as well as the support structure, and the lower zone which consists of the quench. A water-cooled pressure vessel surrounds the reactor, allowing operation up to 0.5 barg. The cylindrical reaction zone in the center is formed by a multilayer coaxial refractory lining that can withstand up to 1800°C. Electric heaters are integrated into the lining, which preheat the reactor before operation. The whole reaction chamber has a length of 2.3 m and a diameter of 250 mm.
On top of the reactor sits a swirl burner consisting of two concentric channels. The outer one supplies the gasification agent while the fuel is fed through the inner channel. The gasification agent is preheated to 300°C and controlled by a mass flow controller (MFC). A pneumatic dense phase conveyor system uses nitrogen as a carrier gas to transport the pulverized feedstock from the storage vessel into the burner. A mass flowmeter determines the amount of nitrogen fed into the reactor, while constant weighing of the feed tank ensures continuous monitoring of the feed rate. The quench sits at the end of

https://doi.org/10.52202/077185-0174

the reaction chamber and rapidly cools down the produced gas by spraying water into the lower part of the vessel. The cooled syngas then leaves the reactor for further treatment.

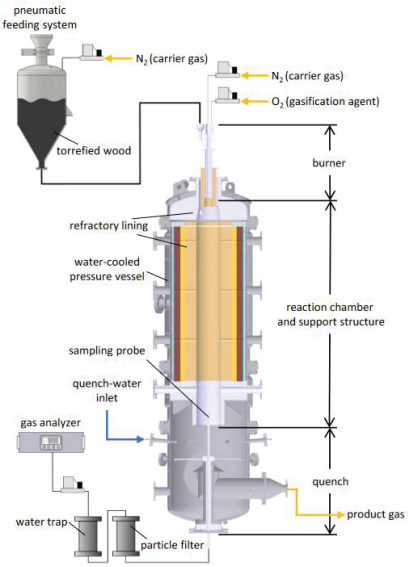

Figure 1: Experimental setup of a vertical entrained-flow gasifier

Mass flow meters measure all gas flows that enter the reactor. Type S thermocouples are placed in a ceramic protection tube and positioned flush with the inner end of the lining. They measure the reaction chamber's internal wall temperature at six positions along the flow direction.

A sampling probe can take gas and particle samples from the reaction zone right above the water quench. The probe is kept at a constant temperature above water vapor saturation via a thermal oil circuit so that the partial water vapor pressure of the product gas can be measured. A sintered metal filter cleans the gas while a water trap cools it. Downstream of the gas cleaning, an MFC controls the gas flow through the probe. From this gas flow, a portion is continuously fed to an extractive gas analyzer that measures the main gas components. Gas composition is measured using non-dispersive infrared absorption for CO_2, CH_4, CO, a thermal conductivity detector for H_2, and a paramagnetic sensor for O_2.

Fuel preparation

Torrefied wood was selected as fuel for the experiments. The feedstock comes from mixed fresh waste wood, which was not debarked. The torrefaction was carried out in a commercial torrefaction plant with a maximum temperature of around 290°C and a total residence time of 45 minutes. The powdered fuel was sieved to 260 µm before use to obtain the desired particle size.

Table 1: Proximate and ultimate analysis of torrefied wood

parameter	value
moisture, %	5.46
ash, %	1.91
volatiles, %	62.10
HHV, kJ/kg	23240
LHV, kJ/kg	23103
C, %	57.88
H, %	6.36
O, %	27.99
N, %	0.36
S, %	0.04

https://doi.org/10.52202/077185-0174

3 MATHEMATICAL MODEL

Plasma-assisted gasification of pulverized biomass fuel is a complex process consisting of many different partial processes, the most important of which are: moisture evaporation, devolatilization, oxidation and reforming of volatiles and biomass char. Depending on the biomass type and process conditions, e.g. the size of the biomass particles and the heating rate, the aforementioned partial processes can either occur simultaneously or follow one after another.

Mathematical model of plasma-assisted gasification of biomass fuel is described by the Euler-Lagrange model, i.e. a model in which the gas medium is treated as a continuous phase and the biomass pulverized fuel is treated as discrete Lagrangian particles moving in the gas medium. The two phases, i.e. the gas phase and the discrete phase, interact with each other by exchanging mass, momentum and energy.

In this work, the steady-state numerical simulations were performed to model reacting turbulent incompressible flow of a viscous fluid using three-dimensional steady Reynolds Averaged Navier-Stokes (RANS) approach. The simulations were carried out using CFD software ANSYS Fluent 2023R1. The numerical setup solved the governing equations for the gas mixture and species mass, momentum, and energy conservation laws, and additionally the equations describing the turbulence model and the radiation transfer equation. The equations are written as follows (Poinsot and Veynante, 2011, Peters 2000):

- mass conservation equation:

$$\nabla \cdot (\rho \boldsymbol{u}) = s_p, \tag{1}$$

  where ρ and $\boldsymbol{u}$ are respectively the mass density and flow velocity, s_p is the mass source from the dispersed phase, e.g. due to moisture evaporation, volatiles release or oxidation and gasification of char,

- momentum conservation equation:

$$\nabla \cdot (\rho \boldsymbol{u}\boldsymbol{u}) = -\nabla p + \nabla \cdot T + \rho \mathbf{g} + \boldsymbol{F}_p\,, \tag{2}$$

  where p is pressure, T is the Reynolds stresses tensor modelled with the SST k-ω turbulence model, $\boldsymbol{F}_p$ is an appropriate interphase gas-particle momentum exchange function,

- gas species conservation equation:

$$\nabla \cdot (\rho \boldsymbol{u} Y_i) = \nabla \cdot \left(\frac{\lambda}{c_p} \nabla Y_i\right) + \omega_i + s_{p,i}\,, \tag{3}$$

  where Y_i is the mass fraction of the i-th species, ω_i and $s_{p,i}$ are the mass source of the i-th species respectively coming from gas phase reactions and from dispersed phase,

- energy conservation equation:

$$\nabla \cdot (\rho \boldsymbol{u} h) = \nabla \cdot \left(\frac{\lambda}{c_p} \nabla h\right) + \omega_h + q_p, \tag{4}$$

  where ω_h is the energy source term due chemical reactions in the gas phase, λ is the thermal conductivity, c_p is the specific heat, q_p is an appropriate interphase energy exchange function.

In the current simulations, the following reactions are considered for the gas phase (Schuster *et al.*, 2001, Mountouris *et al.*, 2006):

- oxidation of volatiles released during devolatilization of biomass fuel:

$$\mathrm{C}_m\mathrm{H}_n\mathrm{O}_l\mathrm{N}_k + (m + n/2 - l)/2\ \mathrm{O}_2 \ \rightarrow\ m\,\mathrm{CO}\ + n/2\ \mathrm{H_2O}\ +\ k/2\ \mathrm{N_2} \tag{5}$$

- water steam reforming (WSR) of volatiles released during devolatilization of biomass fuel:

$$\mathrm{C}_m\mathrm{H}_n\mathrm{O}_l\mathrm{N}_k + (m - l)\mathrm{H_2O}\ \rightarrow\ m\,\mathrm{CO}\ + (m - l + n/2)\ \mathrm{H_2}\ +\ k/2\ \mathrm{N_2} \tag{6}$$

- oxidation of carbon monoxide:

$$\mathrm{CO}\ + 0.5\ \mathrm{O_2}\ \rightarrow\ \mathrm{CO_2} \tag{7}$$

- oxidation of hydrogen:

$$\mathrm{H_2}\ + 0.5\ \mathrm{O_2}\ \rightarrow\ \mathrm{H_2O} \tag{8}$$

- water gas shift reaction (WGSR):

$$\mathrm{CO}\ + \mathrm{H_2O}\ =\ \mathrm{CO_2} + \mathrm{H_2} \tag{9}$$

  that is assumed to be in equilibrium.

https://doi.org/10.52202/077185-0174

The rate of the reactions (5)÷(8) is defined by the approach combining both the Arrhenius finite rate model (FR) and the eddy-dissipation model (ED) as follows:

$$r_i = \min(r_t, r_k)\,, \tag{10}$$

where r_t is the turbulent mixing rate defined for the non-premixed (diffusion) combustion as (Magnussen *et al.*, 1979):

$$r_t = A\frac{\rho}{M_F}\frac{\varepsilon}{k}\min\left(Y_F, \frac{Y_O}{\nu}, B\frac{\sum_P Y_P}{1+\nu}\right) \tag{11}$$

where Y is the mass fraction of oxidizer O, fuel F or product P, $A = 4.0$ and $B = 0.50$ are empirical model parameters, ν is the stoichiometric oxygen to fuel mass ratio, and ε and k are turbulence parameters determined by a turbulence model adequate for the flow conditions.

The Arrhenius rate, r_k, of the k-th reaction is defined as (Poinsot and Veynante, 2011, Peters 2000):

$$r_k = A_k\, T^{n_k}\, e^{-E_k/(RT)} \prod_{i=1}^{i=g} C_{Y_i}^{n_{i,k}} \tag{12}$$

where A is the pre-exponential factor, n is the temperature exponent, E is the activation energy, C is molar concentration of the i-th Y species. Thermodynamic and transport properties of the reacting gas mixture, i.e. specific heat c_p, dynamic viscosity μ, and thermal conductivity λ, were modeled as mass average properties of the main species present in the system. Thermodynamic and transport properties of individual species were computed at the high temperature of plasma condition. (Boulos *et al.*, 2023, McBride *et al.*, 2002, Krenek, 2008, Aubreton *et al.*, 2009). The total mass of the fuel particle, m_p, is defined as follows:

$$m_p(t) = m_a + m_w(t) + m_v(t) + m_C(t), \tag{13}$$

where the individual particle components are mass of ash m_a, moisture m_w, volatiles m_v and carbon m_C. Ash mass remains constant during the process while mass of moisture, volatiles and carbon decreases due to moisture evaporation, volatiles release (devolatilization), oxidation and gasification of char carbon. It was additionally assumed that due to: 1) small biomass particle size (the Rosin-Rammler distribution in the range up to 260 μm with average diameter of 133 μm and polydispersion parameter of 1.55) and 2) the high heating rate (>10^4 K/s) of fuel particles that move through hot plasma, all the individual processes, i.e. moisture evaporation, devolatilization and char carbon gasification, take place at the same time and are activated only depending on the actual particle temperature (Stahlherm *et al.*, 1974). The mass of each k-th fuel component evolves according to the mass conservation equation:

$$\frac{dm_k}{dt} = -r_k, \tag{14}$$

where r_k describes the rate of the specific process that the fuel particle is subjected to, i.e.

- moisture evaporation described by the reaction:

$$\text{moisture}_{(l)} \rightarrow H_2O_{(g)} \tag{15}$$

  where the rate of moisture evaporation r_{ev} is defined as

$$r_{ev} = k_{ev}\, m_w(t) = A_{ev} \exp\left(\frac{-E_{ev}}{RT_p}\right) m_w(t), \tag{16}$$

  where A_{ev}= 5000 1/s and E_{ev}=10 kJ/mol,
- volatiles release (devolatilization) described by the reaction:

$$\text{volatiles}_{(s)} \rightarrow \text{volatiles}_{(g)} \tag{17}$$

  where the rate of devolatilization r_{de} is defines as

$$r_{de} = k_{de}\, m_v(t) = A_{de} \exp\left(\frac{-E_{de}}{RT_p}\right) m_v(t), \tag{18}$$

  where A_{de}= 12000 1/s and E_{de}=32 kJ/mol. Volatiles are represented as one hydrocarbon $C_mH_nO_lN_k$ and values of m, n, l and k follow from the ultimate and proximate analysis of fuel,
- oxidation and gasification of char carbon described by the following reactions:

$$C + 0.5\,O_2 \rightarrow CO, \tag{19}$$
$$C + O_2 \rightarrow CO_2, \tag{20}$$
$$C + H_2O \rightarrow CO + H_2, \tag{21}$$
$$C + CO_2 \rightarrow 2\,CO, \tag{22}$$

https://doi.org/10.52202/077185-0174

where the oxidation rate (reactions 19 and 20) is defined as the diffusion-kinetic limited process:

$$r_{\mathrm{C},i} = \pi d_p^2 M_{\mathrm{C}} \psi_i \frac{k_d k_{c,i} f_s(\mathrm{X_C})}{k_d + f_s(\mathrm{X_C})(k_{c,1} + k_{c,2})} C_{g,\infty} \tag{23}$$

and the gasification rate (reactions 21 and 22) is defined as the kinetic limited process:

$$r_{C,i} = \pi d_p^2 M_{\mathrm{C}} \psi_i k_{\mathrm{C},i} f_s(X_{\mathrm{C}}) C_{g,\infty} \tag{24}$$

with $i = 1$ and $i = 2$ and $g = O_2$ for the reactions (19) and (20), ψ_1= 2mol-C/mol-O_2, ψ_2= 1mol-C/mol-O_2, and with $i = 3$ and $g = H_2O$ for the reaction (21), and $i = 4$ and $g = CO_2$ for the reaction (22), d_p is the particle diameter, M_C=12 kg/kmol, ψ_3= 1mol-C/mol-H_2O, ψ_4= 1mol-C/mol-CO_2, $C_{g,\infty}$ is the mole concentration of the gasification gas reagent in the bulk flow, and

$$k_{\mathrm{C},i} = A_{\mathrm{C},i} \exp\left(\frac{-E_{\mathrm{C},i}}{RT_p}\right) \tag{25}$$

with $A_{C,1}$= $3 \cdot 10^5$ m/s, $E_{C,1}$=180kJ/mol, $A_{C,2}$= 2309 m/s, $E_{C,2}$=113 kJ/mol $A_{C,3}$= $40 \cdot 10^3$ m/s, $E_{C,3}$=240kJ/mol, $A_{C,4}$= $100 \cdot 10^6$ m/s, $E_{C,4}$=270 kJ/mol, and k_d is the mass transfer coefficient:

$$k_d = \frac{Sh\, D}{d_p} \tag{26}$$

where D is the effective diffusion coefficient and Sh is the Sherwood number. Based on the definition of the surface reaction mechanism, it is assumed that the reactive components of the solid phase are constantly available for reaction. However, due to the specific skeletal-porous structure of the solid fuel particle, the availability of reactive solid-phase components depends on their degree of conversion (depletion level). The model assumes that the availability of the k-th solid-phase component for the surface reaction is defined by the f_s function describing the relative change in the active surface area during the surface reaction (Baum and Street, 1971). The form of the f_s function should be determined from experimental results. However, due to the complicated and difficult process of measuring the active surface area during the gasification process, the following simple form is usually adopted for calculation purposes (Lewtak and Milewska, 2013, Hercog, 2014):

$$f_s(\mathrm{X_C}(t)) = (1 - \mathrm{X_C}(t))^q \tag{27}$$

where q=1.65 is a model parameter (Stahlherm *et al.*, 1974), and

$$\mathrm{X_C}(t) = \frac{m_{\mathrm{C},0} - m_{\mathrm{C}}(t)}{m_{\mathrm{C},0}} \tag{28}$$

is the char carbon burnout.

Each of the k equations (14) is solved with the following initial condition:

$$m_k(t=0) = f_{k,0}\, V_{p,0} \left(\sum_{k=1}^{k=4} \frac{f_{k,0}}{\rho_k}\right)^{-1}, \tag{29}$$

where $f_{k,0}$ is the initial mass fraction of the k-th particle component that has density of ρ_k, $V_{p,0}$ is the initial particle volume that change during the process as:

$$V_p(t) = V_{p,0}(1 - \mathrm{X}_p(t))^{\alpha} \tag{30}$$

with α=1 was assumed (Smith, 1982, Hamor *et al.*, 1973) and

$$\mathrm{X}_p(t) = \frac{m_{p,0} - m_p(t)}{m_{p,0}} \tag{31}$$

is the total particle burnout. The particle density is then defined as:

$$\rho_p(t) = \frac{m_p(t)}{V_p(t)}, \tag{32}$$

and unlike other models that maintain a constant particle volume during the gasification process, the current approach considers the changes of particle volume due to the particle burnout, that protects the particle density from excessive reduction.

The particle temperature is determined as the solution of the equation describing the law of conservation of energy for a particle as follows:

$$m_p(t) c_p \frac{dT_p}{dt} = h^* A_p \left(T_{f,\infty} - T_p(t)\right) + A_p \varepsilon_p \sigma \left(T_{f,\infty}^4 - T_p^4(t)\right) + \sum_i r_i(t) \Delta H_i \tag{33}$$

https://doi.org/10.52202/077185-0174

where ΔH_i is the heat of the i-th surface reaction (R1) or (R2), and moisture evaporation. The heat transfer coefficient h^*, that considers simultaneous exchange of mass and heat between a particle and its gaseous surroundings, is defined as (Taylor and Krishna, 1993, Baehr and Stephan, 2006):

$$h^* = h\,\Psi, \tag{34}$$

where

$$h = \frac{k_{f,\infty}}{d_p}\,\mathrm{Nu} \tag{35}$$

is the heat transfer coefficient (without mass exchange),

$$\mathrm{Nu} = 2 + 0.6\,\mathrm{Re}_p^{0.5}\,\mathrm{Pr}^{0.33} \tag{36}$$

is the Nusselt number. The coefficient Ψ, correcting the heat transfer coefficient, is defines as

$$\Psi = \frac{\Phi}{e^{\Phi} - 1} \tag{37}$$

where the nondimensional heat transfer coefficient Φ is expressed as:

$$\Phi = \frac{r_{ev} + r_{de} + r_{\mathrm{C}}}{4\pi r_p \rho_p D}. \tag{38}$$

The gas and dispersed phase coupling is accomplished by alternately solving the steady-state continuous and unsteady dispersed phase equations until the solutions in both phases have stopped changing. The biomass gasification model presented above was implemented into Ansys Fluent using available user functions (so-called UDF). Other equations, describing the processes in the gas phase, were solved using the coupled algorithm available in Fluent with second order discretization method. The SST k-ω model was used to describe the turbulent flow of the gas medium. The discrete-ordinates method was used to solve the radiation transfer equation (RTE) describing the radiation heat transfer and the weighted-sum-of-gray-gases model (WSGG) was applied for the emissivity of the gas phase.

4 RESULTS AND DISCUSSION

This section presents the results of numerical modelling of the plasma-assisted biomass gasification process in the vertically entrained flow gasifier. In real plasma gasification conditions, at which fuel particles are quickly heated (the high heating rate at around 10^4-10^5K/s depending on the particle diameter compared to the low heating rate at around $1 \div 10^2$K/s at ultimate analysis), the volatile yield is significantly higher than what the proximate analysis of the fuel would indicate. The maximum volatile release that can be released is known as the so-called high volatile yield (HVY). Additionally, in literature the Q factor is often used instead of the HVY to characterize the devolatilization behavior under high rate heating conditions, so that the Q factor is defines as (Becker *et al*., 2017):

$$\mathrm{Q} = \frac{\mathrm{HVY}}{\mathrm{VY}} \tag{39}$$

where HVY and VY are volatile yields respectively received at high and low heating rate that meet conditions of authentic industrial processes and proximate analysis/TGA, respectively. Thus, the kinetic parameters of devolatilization derived from TGA (max heating rate of 1 K/s) may not apply in industrial applications (Niemelä *et al*., 2021) and to overcome this issue usually drop-tube reactors are involved. In this study, attempts were made to study the influence of different volatiles yield on the overall gasification process. Numerical calculations were carried out for 5 various values of high volatile yield (different values of the Q factor), starting from the value of Q=1 (corresponding to low heating rate conditions), and ending with the maximum value, for which all fixed carbon is released in the form of volatiles. It should also be considered that different amounts of volatiles released (depending on the heating rate and the particle size) not only affect the gasification process quantitatively, but also qualitatively, because the C/H ratio of volatiles released increases with an increase of volatile yield. Table 2 presents the selected boundary conditions used in the numerical simulations. For all cases, the plasma temperature, mass flow rate and thermal power were 3200 K, 2.18 g/s and 30 kW, respectively. The plasma was composed of 85%m H_2O and 15%m Ar. Biomass fuel of 15 kg/h, carried by the nitrogen stream of 1.66 kg/h, was fed into the reactor by 2 inlets for all cases. In addition, a gas mixture of 79%v O_2 and 21%v H_2O steam was fed at the mass flow rate 3.05 kg/h at 373 K below the fuel inlets (v. Fig. 2). Along the reactor wall, the Dirichlet boundary conditions were applied for temperature,

https://doi.org/10.52202/077185-0174

starting at 1700K on the reactor diffuser and ending at 1300K on the reactor bottom. Figure 2 shows the geometric model of the plasma-assisted gasifier used for the CFD calculations. The overall height of the gasifier is 2300 mm and the inner diameter of the vertical reactor section is 250 mm. The main components of the gasifier are:

- thermal arc plasma torch (located on the top of the gasifier), electrically generating arc plasma from a mixture of Ar and H_2O,
- diffuser (located below the plasma torch), with built in of 2 levels of inlets. Through the inlets of level 1, located closer to the plasma burner, fuel (biomass) is supplied together with a carrier gas (N_2) by 2 inlets located opposite each other, and through the inlets of level 2 an additional reaction gas (mixture of O_2 and H_2O) for the gasification process was supplied by 4 inlets,
- the gasification reactor (located below the diffuser) in which the gasification process takes place.

Table 2. Fuel proximate composition applied in CFD

process parameter	case 1	case 2	case 3	case 4	case 5
Q factor	**1.00**	**1.10**	**1.25**	**1.40**	**1.49**
moisture, %	5.46	5.46	5.46	5.46	5.46
ash, %	1.91	1.91	1.91	1.91	1.91
volatiles, %	62.10	68.31	77.63	86.94	92.63
fixed carbon, %	30.53	24.32	15.00	5.69	0.00
C/H ratio for volatiles	0.358	0.440	0.562	0.684	0.758

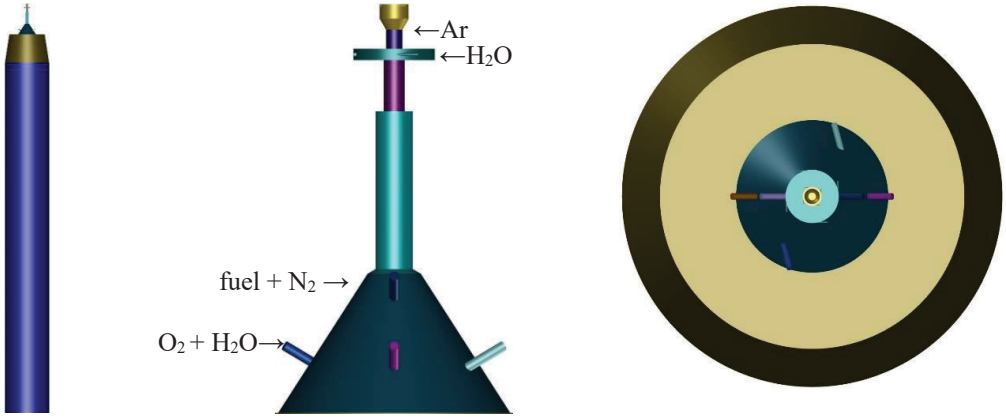

a) reactor b) details of the plasma torch c) top view

Figure 2. Geometry definition of the CFD model

Figures 3, 4, and 5 show selected numerical results, i.e. contours of velocity, temperature, mole fractions of H_2, CO, CO_2 and H_2O for the cases 2, 3 and 4. The contours are shown in two vertical cross sections mutually perpendicular to each other. It is noteworthy that the gasification process is qualitatively similar across all computational cases, especially with regard to the profiles of CO, H_2, H_2O and CO_2 (Fig. 3, 4, 5), and the occurring quantitative differences in gas concentrations result from the different yield of volatiles released during devolatilization according to the Q value used. Biomass particles flow directly adjacent to or through the plasma jet, and subsequently undergo significant heating rate of 10^4-10^5 K/s depending on the particle diameter. Regardless of the scenario, the two inlets of biomass are aligned in such a way as to guide the fuel particles through the intensely hot plasma jet, that results in evaporation of moisture and the release of volatiles as the biomass temperature rises. Due to the presence of water vapour and the immediate surroundings of the hot H_2O-Ar plasma jet, the released volatiles, which may include tars and hydrocarbons, rapidly undergo WSR reaction to produce CO and H_2 (eq. 21). O_2, supplied together with H_2O through the inlets on the diffuser, is quickly and completely consumed near the diffuser zone for the oxidation reactions of volatiles and CO, and therefore the O_2

https://doi.org/10.52202/077185-0174

concentration in the reactor chamber is zero. In the current reactor operational conditions, CO_2 is also formed by the WGSR. In addition to the oxidation reaction of CO, in proximity to the burner, negligible amounts of CO_2 are generated also due to the WGSR (eq. 9), even if it has a small equilibrium constant (K<1) at high temperature, causing the reaction equilibrium to shift towards the left side, whereby CO and H_2O are favored. Furthermore, low concentrations of CO_2 (below 10%v) do not activate the gasification reaction 22, wherein the primary role is fulfilled by the gasification of char coal with water steam in the reaction 21. CO_2 combined with H_2 are solely produced in the WGSR within the outlet section of the reactor, where the temperature is lower and the equilibrium constant of the WGSR attains higher values. In all cases, the plasma jet is swirled at the torch outlet and the stream of particles and N_2, after colliding with the plasma jet, forms characteristic swirl structures (top views, Fig. 3,4,5).
Finally, Table 3 shows the most important performance parameters of gasification, i.e. syngas composition and heating value, cold gas efficiency, the mass flow rate and power of syngas at the gasifier outlet. H_2 and CO content in the syngas increases with increasing value of Q. Increasing content of H_2 is a result of the WSR reaction, in which volatiles and H_2O are consumed exactly to create high amount of H_2. Therefore, in addition to moisture evaporated from biomass fuel, it is important to provide sufficient amount of H_2O into the gasifier to ensure high conversion of volatiles.
The cold gas efficiency (CGE) of the gasifier is defined as the ratio between the chemical energy of the produced syngas (obtained as syngas flow rate Q_{sg} multiplied by its net heating value LHV_{sg}) and the chemical energy of the fuel fed to the gasifier (obtained as fuel flow rate Q_{fm} multiplied by its net heating value LHV_{fm}) (Liao *et al.*, 2021; Guo *et al.*, 2023):

$$\mathrm{CGE} = \frac{\mathrm{Q_{sg}} \cdot \mathrm{LHV_{sg}}}{\mathrm{Q_{fm}} \cdot \mathrm{LHV_{fm}}}. \tag{40}$$

It is interesting to observe that the CGE noticeably increases as Q increases that is indeed due to increasing both mass flow rate of syngas and fractions of H_2 and CO in the syngas. However, the most interesting result is that the CGE can reach values greater than 100% (case 4 and case 5) due to increase of H_2 syngas content coming from the water vapor at the WSR reaction.

Table 3. Parameters of the syngas achieved at the gasifier outlet

parameter	case 1	case 2	case 3	case 4	case 5
H_2, %v	38.96	41.16	43.73	45.64	46.50
CO, %v	19.11	23.61	30.24	36.78	40.24
CO_2, %v	7.20	6.42	4.88	2.81	1.61
H_2O, %v	27.17	21.82	14.92	9.17	6.28
T, K	1323	1347	1389	1525	1738
LHV, MJ/kg	8.94	10.1	11.9	13.5	14.3
Q_{sg}, kg/h	23.0	23.7	25.2	26.5	27.3
P_{sg}, kW	57.1	66.6	83.5	99.4	109
CGE, %	59.3	69.2	86.8	103	113

5 CONCLUSIONS

A mathematical model of the plasma-assisted gasification process has been developed and applied to study the gasification process of torrefied biomass in a vertical entrained-flow plasma-assisted gasifier. The numerical simulations were mainly used to investigate the influence of the Q factor (volatiles yield) on the quality of the syngas obtained at the reactor outlet and the course of the process inside the reactor. Due to the high heating rate of the fuel, a high volatile yield was achieved, which can sum up most of the fixed carbon. Then, in the steam reforming reaction, the volatiles released are converted into CO and H_2. The gasification reactor acts as a reactor for the steam reforming of the volatiles and the gasification of the char carbon remaining as fixed coal. The syngas produced is of high quality (high concentrations of H_2 = 44%v wb. and CO = 30%v wb) and high purity due to the absence of problematic tars and hydrocarbons, which is a characteristic feature of plasma-assisted gasification. The high value of the cold gas efficiency was achieved as 70÷80% depending on the Q value applied.

https://doi.org/10.52202/077185-0174

https://doi.org/10.52202/077185-0174

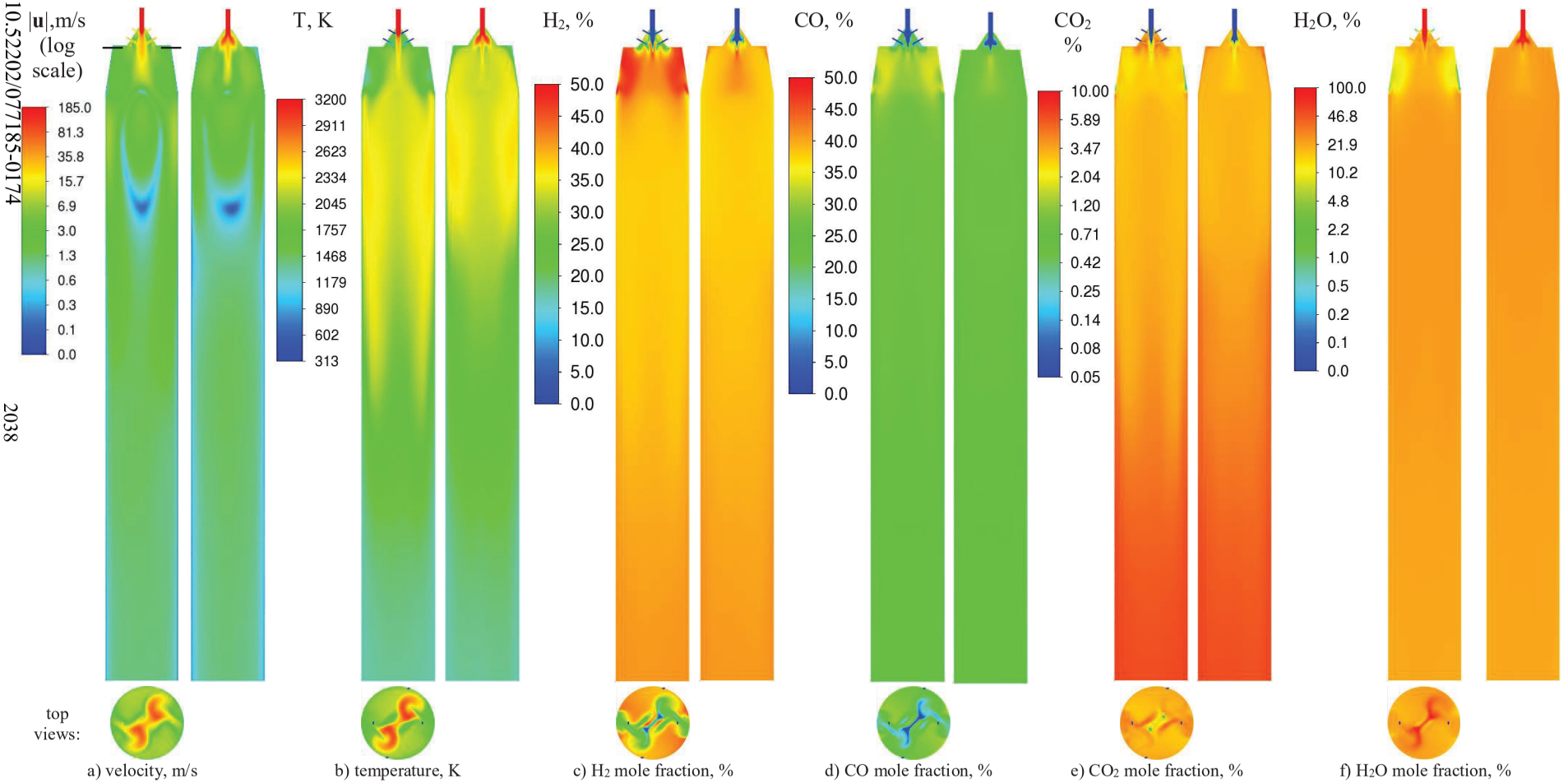

Figure 3. Selected numerical results for the case 2 (Q = 1.10)

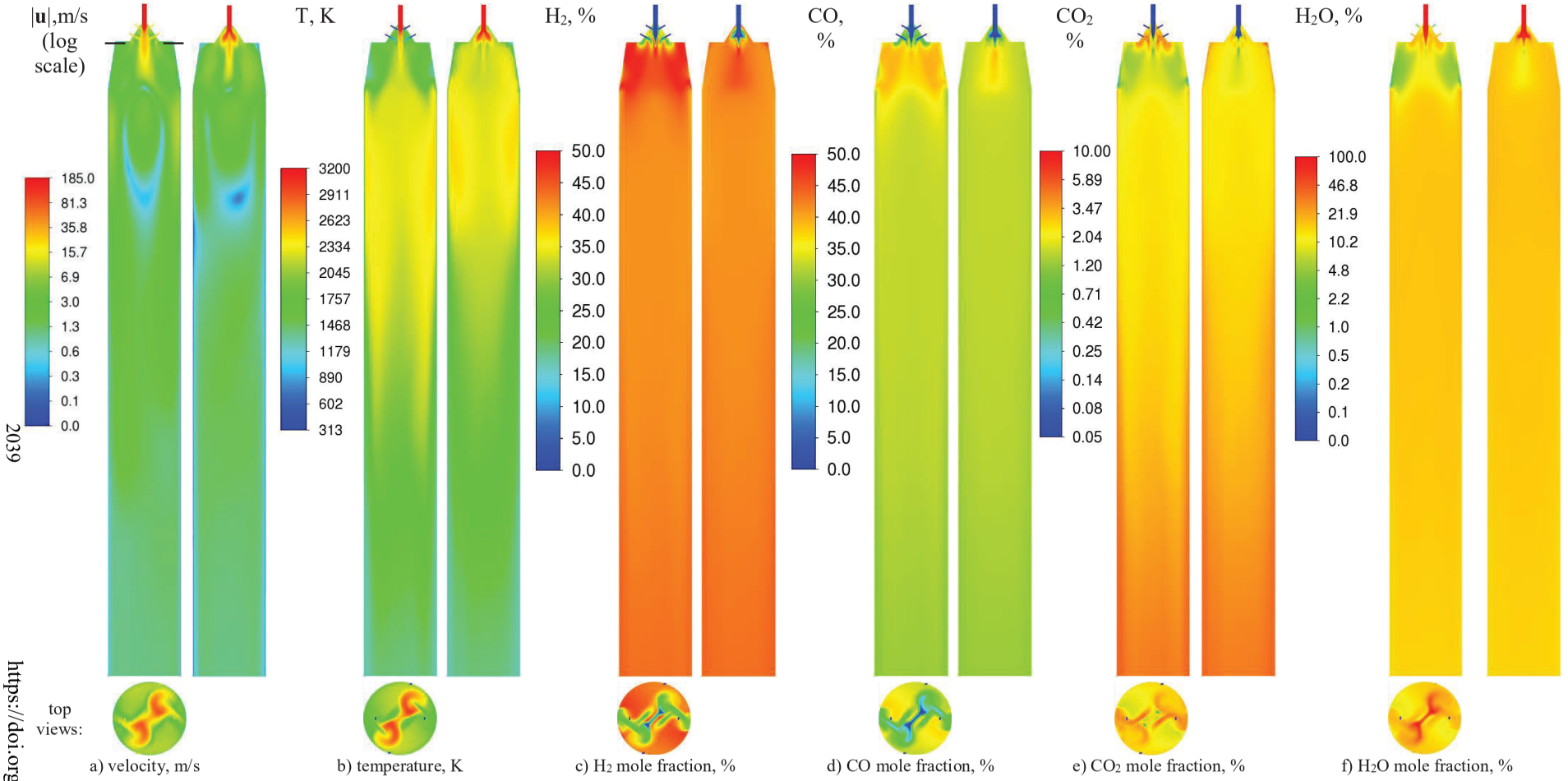

Figure 4. Selected numerical results for the case 3 (Q = 1.25)

2039
https://doi.org/10.52202/077185-0174

https://doi.org/10.52202/077185-0174

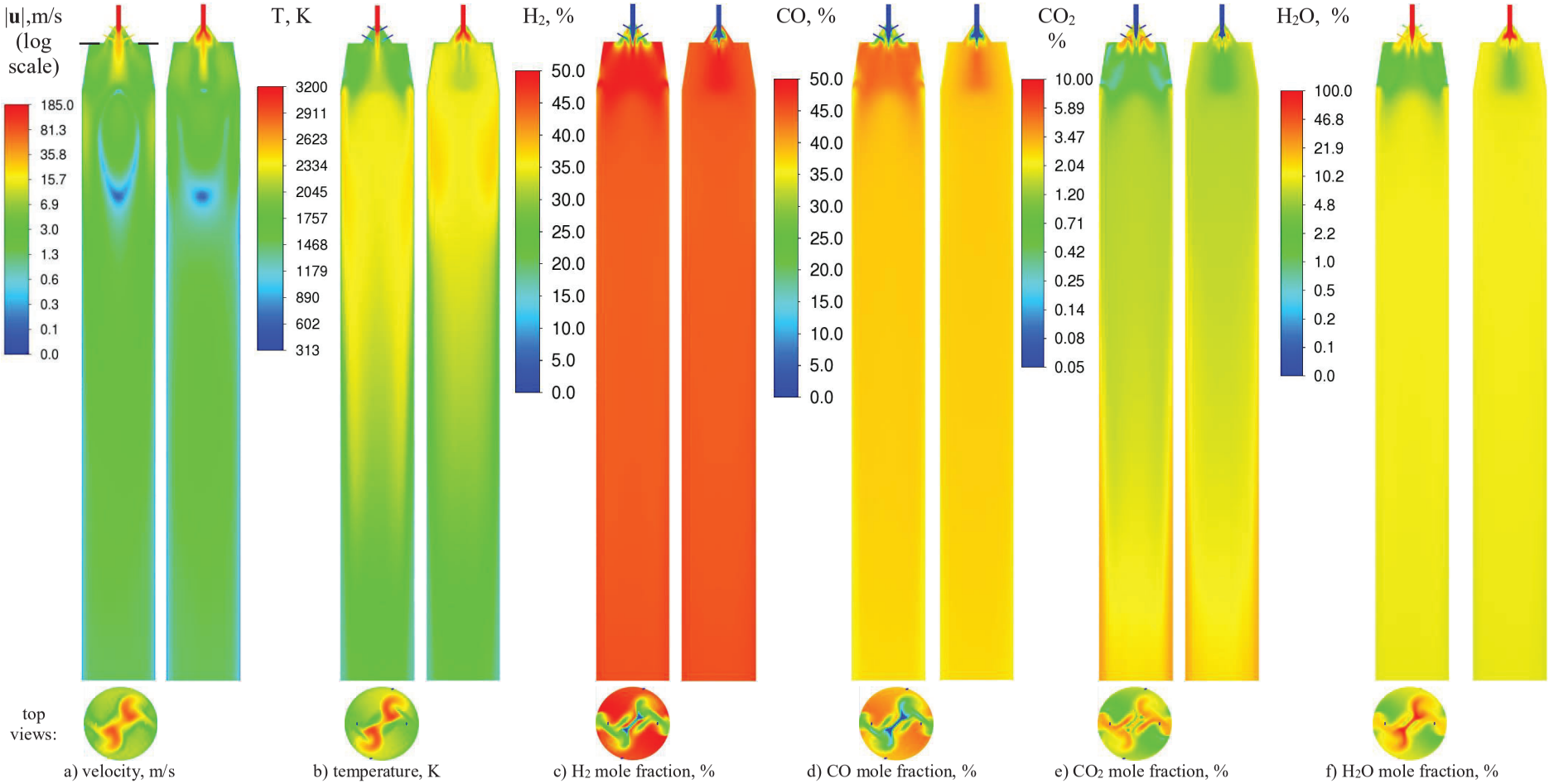

Figure 5. Selected numerical results for the case 4 (Q = 1.40)

REFERENCES

Aubreton, J., Elchinger, M.F., Vinson, J.M., 2009, Transport coefficients in water plasma: Part I: Equilibrium plasma, Plasma Chem Plasma Process, vol. 29, p. 149–171.

Baehr, H.D., Stephan, K., 2006, Heat and mass transfer, 2nd ed. Springer; . p. 688.

Baum, M.M., Street, P.J., 1971, Predicting the combustion behaviour of coal particles, Combustion Science and Technology, vol. 3(5), p. 231-243.

Becker, A., Schiemann, M., Scherer, V., Shaddix, C., Haxter, D., Mayer, J., 2017, Comparative ignition tests of coal under oxy-fuel conditions in a standardized laboratory test rig, Fuel, 208, p. 127-136.

Boulos, M.I., Cressault, Y., Fauchais, P.L., Murphy, A.M., Pfender, M., 2023, Thermodynamic and transport properties of gases over the temperature range 300-30000 K., in Handbook of thermal plasmas, ed.: Boulos M.I., Fauchais P.L., Pfender M, Springer, p. 1975.

Guo, Q., Li, R., Yang, G., Liu, Y., Deng, Q., He, Z., 2023, Experimental study on a small-scale oxygen-enriched entrained flow biomass gasifier assisted by non-thermal arc plasma, *Energy Reports*, vol. 9, p. 4298-4305.

Hamor, R.J., *et al*., 1973, Kinetics of combustion of a pulverized brown coal char between 630 and 2200 K, Combust Flame, vol. 21, p.153-162.

Hercog, J., Lewtak, R., 2014, Experimental and numerical investigation of coal char combustion process under standard and oxy-fuel conditions, Proc. of the 39th International Technical Conference on Clean Coal & Fuel Systems, Clearwater, USA, p. 198-209.

Krenek, P., 2008, Thermophysical properties of H_2O–Ar plasmas at temperatures 400–50000 K and pressure 0.1 MPa, Plasma Chem Plasma Process, vol. 28, p. 107–122.

Lewtak, R., Milewska, A., 2013, Application of different diffusion approaches in oxy-fuel combustion of single coal char particles, Fuel, vol. 113, p. 844-853.

Liao, L., Zheng, J., Zhang, Y., Li, C., Yuan, C., 2021, Impact of torrefaction on entrained-flow gasification of pine sawdust: An experimental investigation, *Fuel*, vol.~298, p. 119919.

Magnussen, B.F., Hjertager, B.H., Olsen, J.G., Bhaduri, D., 1979, Effects of turbulent structure and local concentrations on soot formation and combustion in C_2H_2 diffusion flames, Symposium (Int.) Combustion, vol. 17(1), p. 1383–1393.

McBride, B.J, Zehe, M.J., Gordon, S., 2002, NASA Glenn coefficients for calculating thermodynamic properties of individual species, NASA/TP—2002-211556, Glenn Research Center, p. 286.

Mountouris, A., Voutsas, E., Tassios, D., 2006, Solid waste plasma gasification: Equilibrium model development and exergy analysis, Energy Conversion and Management, vol. 47, p. 1723–1737.

Niemelä, N.P., Delgado, R.N., de Riese, T., Tolvanen, H., Fendt, S., Spliethoff, H., Joronen, T., 2021, Fuel-specific devolatilization parameters for detailed comparison of pulverized biomass fuels, *Fuel*, vol. 286, p.119309.

Peters, N., 2000, Turbulent combustion, Cambridge University Press, 304 p.

Poinsot, T., Veynante, D., 2011, Theoretical and numerical combustion, Edwards, 3rd ed. 522 p.

Schuster, G., Löffler, G., Weigl K., Hofbauer H., 2001, Biomass steam gasification - an extensive parametric modeling study, Bioresource Technology, vol. 77, p. 71-79.

Smith, I.W., 1982, The combustion rates of coal chars: A review, Symposium (Int.) on Combustion, vol. 19(1), p. 1045-1065.

Stahlherm, D., Jüntgen, H., Peters, W., 1974, Zündmechanismus und Abbrand von Kohlekörnern. Erdöl und Kohle -Erdgas – Petrochemie, vol. 27(2), p. 64–70.

Taylor, R, Krishna, R., 1993, Multicomponent mass transfer, John Wiley & Sons Inc.; p. 616.

ACKNOWLEDGEMENT

This study was carried out in the framework of the International Future Lab on Green Hydrogen Technologies “REDEFINE Hydrogen Economy (H2E)” (project no.: 01DD21005) sponsored by the Federal Ministry for Education and Research (Germany). The financial support is gratefully acknowledged.

https://doi.org/10.52202/077185-0174